Vibrational imaging of newly synthesized proteins in live cells by stimulated Raman scattering microscopy

Lu Wei[a], Yong Yu[b,c], Yihui Shen[a], Meng C. Wang[b,c,1], and Wei Min[a,d,1]

[a]Department of Chemistry and [d]Kavli Institute for Brain Science, Columbia University, New York, NY 10027; and [b]Department of Molecular and Human Genetics and [c]Huffington Center on Aging, Baylor College of Medicine, Houston, TX 77030

Edited by David A. Tirrell, California Institute of Technology, Pasadena, CA, and approved May 31, 2013 (received for review February 27, 2013)

Synthesis of new proteins, a key step in the central dogma of molecular biology, has been a major biological process by which cells respond rapidly to environmental cues in both physiological and pathological conditions. However, the selective visualization of a newly synthesized proteome in living systems with subcellular resolution has proven to be rather challenging, despite the extensive efforts along the lines of fluorescence staining, autoradiography, and mass spectrometry. Herein, we report an imaging technique to visualize nascent proteins by harnessing the emerging stimulated Raman scattering (SRS) microscopy coupled with metabolic incorporation of deuterium-labeled amino acids. As a first demonstration, we imaged newly synthesized proteins in live mammalian cells with high spatial–temporal resolution without fixation or staining. Subcellular compartments with fast protein turnover in HeLa and HEK293T cells, and newly grown neurites in differentiating neuron-like N2A cells, are clearly identified via this imaging technique. Technically, incorporation of deuterium-labeled amino acids is minimally perturbative to live cells, whereas SRS imaging of exogenous carbon–deuterium bonds (C–D) in the cell-silent Raman region is highly sensitive, specific, and compatible with living systems. Moreover, coupled with label-free SRS imaging of the total proteome, our method can readily generate spatial maps of the quantitative ratio between new and total proteomes. Thus, this technique of nonlinear vibrational imaging of stable isotope incorporation will be a valuable tool to advance our understanding of the complex spatial and temporal dynamics of newly synthesized proteome in vivo.

stable isotope labeling | stimulated Raman microscopy | protein synthesis

The proteome of a cell is highly dynamic in nature and tightly regulated by both protein synthesis and degradation to actively maintain homeostasis. Many intricate biological processes, such as cell growth, differentiation, diseases, and response to environmental stimuli, require protein synthesis and translational control (1). In particular, long-lasting forms of synaptic plasticity, such as those underlying long-term memory, require new protein synthesis in a space- and time-dependent manner (2–4). Therefore, direct visualization and quantification of newly synthesized proteins at a global level are indispensable to unraveling the spatial–temporal characteristics of the proteomes in live cells.

Extensive efforts have been devoted to probing protein synthesis via fluorescence contrast. The inherent fluorescence of green fluorescent protein (GFP) and its genetic encodability allow one to follow a given protein of interest inside living cells with high spatial and temporal resolution (5, 6). However, GFP tagging through genetic manipulation works only on individual proteins but not at the whole-proteome level. To probe newly synthesized proteins at the proteome level, a powerful technique named bioorthogonal noncanonical amino acid tagging (BONCAT) was developed by metabolic incorporation of unnatural amino acids containing reactive chemical groups such as azide or alkyne (7–13). A related labeling method was recently demonstrated using an alkyne analog of puromycin (14). Newly synthesized proteins can then be visualized through subsequent conjugation of the reactive amino acids to fluorescent tags via click chemistry (15). Unfortunately, these fluorescence-based methods generally require nonphysiological fixation and subsequent dye staining and washing.

In addition to fluorescence tagging, radioisotope or stable isotope labeling is another powerful tool to trace and quantify proteome dynamics. Classical radioisotope-labeled amino acids (e.g., [^{35}S]methionine) provide vigorous analysis of global protein synthesis. However, samples must be fixed and then exposed to film for autoradiography. For stable isotopes, the discovery of deuterium by Urey in 1932 immediately led to the pioneer work of Schoenheimer and Rittenberg studying intermediary metabolism (16, 17). To study proteome changes between different cells or under different conditions, stable isotope labeling by amino acids in cell culture (SILAC) coupled with mass spectrometry (MS) has matured into a popular method for quantitative proteomics (18–21). However, SILAC-MS does not usually provide spatial information down to subcellular level and its invasive nature also limits its application for live-cell imaging. The same limitation applies to the recent ribosome profiling study using deep sequencing technique (22).

Therefore, it is highly challenging and desirable to be able to quantitatively image proteome synthesis in live cells with high spatial–temporal resolution. Herein, we report using stimulated Raman scattering (SRS) microscopy, an emerging vibrational imaging technique, for the visualization of nascent proteins in live cells coupled through metabolic incorporation of deuterium-labeled amino acids (Fig. 1). Newly synthesized proteins are imaged via their unique vibrational signature of carbon–deuterium bonds (C–D). Vibrational imaging by Raman contrast is a rapidly growing field. Spontaneous Raman microscopy can offer spatially resolved chemical information based on the vibration frequencies of characteristic chemical bonds. However, spontaneous Raman scattering is an intrinsically weak process, hence not ideal for fast live-cell imaging (23). As a nonlinear technique, coherent anti-Stokes Raman scattering (CARS) offers much higher imaging speed by virtue of coherent amplification (24–28). Unfortunately, CARS suffers from spectral distortion, unwanted nonresonant background, nonstraightforward concentration dependence, and coherent image artifact (25). Most recently, SRS microscopy has emerged to supersede CARS microscopy in almost all aspects (29–38). Using Einstein's stimulated emission principle (39, 40), SRS has achieved unprecedented sensitivity down to ~1,000 retinoic acid molecules and up to video rate imaging speed in vivo (30, 33). Unlike CARS, SRS microscopy exhibits straightforward image interpretation and quantification without complications from the nonresonant background and phase-matching conditions (41, 42). Consequently, not only is the signal-to-noise ratio improved over CARS, but the Raman spectral fidelity is

Author contributions: L.W., M.C.W., and W.M. designed research; L.W., Y.Y., and Y.S. performed research; L.W. analyzed data; and L.W., Y.Y., Y.S., M.C.W., and W.M. wrote the paper.

Conflict of interest statement: Columbia University has filed a patent application based on this work.

This article is a PNAS Direct Submission.

[1]To whom correspondence may be addressed. E-mail: wm2256@columbia.edu or wmeng@bcm.edu.

This article contains supporting information online at www.pnas.org/lookup/suppl/doi:10.1073/pnas.1303768110/-/DCSupplemental.

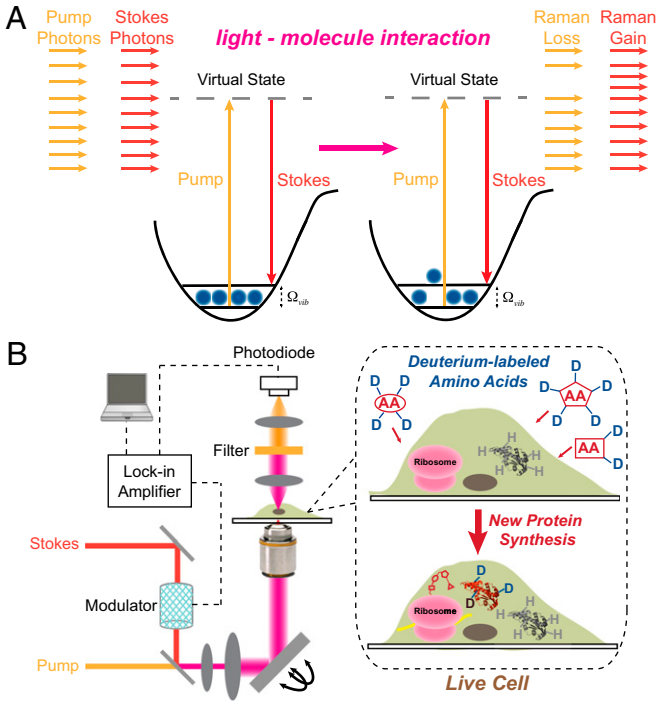

Fig. 1. Stimulated Raman scattering (SRS) microscopy principle and experimental scheme. (*A*) Principle of SRS microscopy. When the energy difference between the Pump beam photon and the Stokes beam photon matches the vibrational frequency (Ω_{vib}) of a specific chemical bond, a molecule is efficiently driven from the vibrational ground state to its vibrational excited state, passing through a virtual state. A quanta of such vibrational activation results in a photon in the Pump beam being annihilated (stimulated Raman loss) and a photon in the Stokes beam being created (stimulated Raman gain), which serves as the contrast for SRS microscopy. (*B*) Experimental scheme of imaging proteins with metabolic incorporation of deuterium-labeled amino acids. By feeding live cells with deuterium-labeled amino acids, newly synthesized proteins can be specifically labeled with carbon–deuterium bonds (C–D). By tuning the energy difference between Pump and Stokes beams to match the vibrational frequency of C–D, the distribution of C–D carrying new proteins can be imaged in live cells by SRS with high sensitivity and resolution without additional fixation or staining.

also preserved and a linear concentration dependence is strictly followed (30).

First, we demonstrated the proof-of-concept of our technique on live HeLa cells using a single deuterium-labeled essential amino acid, leucine-d_{10}. Then we optimized the incorporation efficiency of the deuterium isotope into nascent proteins and showed broad applicability of the method on several mammalian cell lines, particularly, its unique advantage in generating spatial maps of the quantitative ratio between new and old proteomes. Furthermore, besides visualizing newly synthesized proteins in cell bodies, the ability to image nascent proteins in neurites of neuron-like mouse neuroblastoma Neuro-2A (N2A) cells upon differentiation was also shown, demonstrating the prospect of studying de novo protein synthesis during neuronal plasticity, such as long-term memory.

Results and Discussion

Physical Principle of Isotope-Based SRS Imaging. SRS microscopy is a molecular-contrast, highly sensitive imaging technique with intrinsic 3D sectioning capability. It selectively images the distribution of molecules that carry a given type of chemical bonds through resonating with the specific vibrational frequency of the targeted bonds (30, 33, 41). As Fig. 1*A* illustrates, by focusing both temporally and spatially overlapped Pump and Stokes laser pulse trains into samples, the rate of vibrational transition is greatly amplified by about 10^7 times when the energy difference of the two laser beams matches the particular chemical bond vibration, Ω_{vib} (41). Accompanying such stimulated activation of one vibrational mode, one photon is created into the Stokes beam and simultaneously another photon is annihilated from the Pump beam, a process called stimulated Raman gain and stimulated Raman loss, respectively. Essentially, the energy difference between the Pump photon and the Stokes photon is used to excite the vibrational mode, fulfilling energy conservation. As shown in Fig. 1*B*, a high-frequency modulation scheme, where the intensity of the Stokes beam is turned on and off at 10 MHz, is used to achieve shot noise-limited detection sensitivity by suppressing laser intensity fluctuations occurring at low frequencies. The transmitted Pump beam after the sample is detected by a large-area photodiode, and the corresponding stimulated Raman loss signal, which also occurs at 10 MHz, is demodulated by a lock-in amplifier. By scanning across the sample with a laser-scanning microscope, a quantitative map with chemical contrast can be produced from the targeted vibrating chemical bonds. As the SRS signal is dependent on both Pump and Stokes laser beams, the nonlinear nature herein provides a 3D optical sectioning ability.

Here, we detect the vibrational signal of C–D as an indicator for newly synthesized proteins that metabolically incorporate deuterium-labeled amino acids (Fig. 1*B*). When hydrogen atoms are replaced by deuterium, the chemical and biological activities of biomolecules remain largely unmodified. Intriguingly, the C–D stretching motion displays a distinct vibrational frequency from all of the other vibrations of biological molecules inside live cells. It is known from classical mechanics that the frequency of vibrational oscillation, Ω_{vib}, inversely scales with the square root of the reduced mass of the oscillator $\Omega_{vib} = (1/2\pi)\sqrt{k/\mu}$, where k is the spring constant of the corresponding chemical bond, and μ denotes the reduced mass of the oscillator. The reduced mass of the C–D oscillator is increased by two folds when hydrogen is replaced by deuterium. Based on the above equation, Ω_{vib} would be reduced by a factor of $\sqrt{2}$. Indeed, the experimentally measured stretching frequency is shifted from ~2,950 cm^{-1} of C–H to ~2,100 cm^{-1} of C–D. Remarkably, the vibrational frequency of 2,100 cm^{-1} is located in a cell-silent spectral window in which no other Raman peaks exist (Fig. S1), thus enabling detection of exogenous C–D with both high specificity and sensitivity.

SRS Imaging of Newly Synthesized Proteins by Metabolic Incorporation of Leucine-d_{10} in Live HeLa Cells. Among the 20 natural amino acids, leucine is an essential one with both high abundance in protein (~9% in mammalian cells) and a large number of side-chain C–H that can be replaced by C–D (43). Hence, we first demonstrated the feasibility of our technique by detecting the metabolic incorporation of leucine-d_{10} (L-leucine-2,3,3,4,5,5,5,5′,5′,5′-d_{10} as shown in Fig. 2*A*) to nascent proteins in live HeLa cells. Fig. 2*B* shows the spontaneous Raman spectrum of HeLa cells incubated in the medium containing 0.8 mM free leucine-d_{10} for 20 h (blue) overplotted with the spectrum of HeLa cells growing in the regular medium without leucine-d_{10} (red) as well as the spectrum from a 10 mM free leucine-d_{10} solution in PBS (black). As indicated by the comparison between the blue and the red spectra, the Raman peaks of leucine-d_{10}, exhibiting multiple peaks around 2,100 cm^{-1} due to symmetric and asymmetrical C–D stretching, are indeed located in the cell-silent region. The comparison of the blue and the black spectra implies that leucine-d_{10} incorporated into cellular proteome after 20 h is enriched to about 10 mM. Thus, a 10% incorporation yield of leucine-d_{10} can be estimated at this condition based on the intrinsic leucine concentration of about 100 mM in proteins (calculated from protein concentration and leucine percentage in cells).

Based on the above spectra, we choose to target the central 2,133 cm^{-1} vibrational peak of C–D to acquire SRS images of nascent proteins in live HeLa cells. As expected, HeLa cells growing in regular medium show no detectable SRS contrast at 2,133 cm^{-1} (Fig. 2*C*), which is consistent with the flat spectral baseline (red in Fig. 2*B*) in the cell-silent region. In contrast, SRS image of HeLa cells growing in the medium containing 0.8 mM

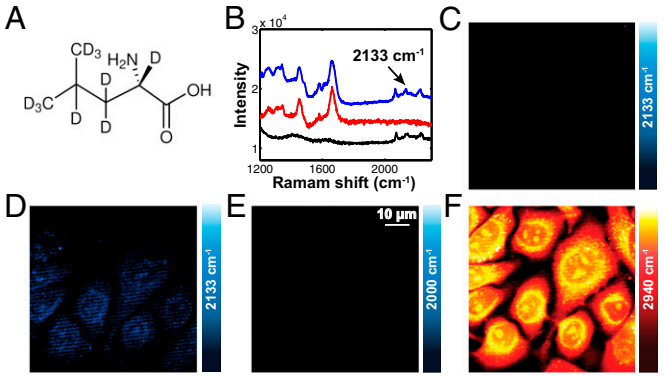

Fig. 2. SRS imaging of newly synthesized proteins by metabolic incorporation of leucine-d_{10} in live HeLa cells. (*A*) Structure of leucine-d_{10} with 10 nonexchangeable side-chain deuterium. (*B*) Spontaneous Raman spectra of HeLa cells incubated with medium containing leucine-d_{10} (0.8 mM) for 20 h (blue), HeLa cells growing in regular medium (red), and 10 mM leucine-d_{10} in PBS solution (black). The C–D Raman peaks lie in the cell-silent region where no Raman peaks from other biological molecules exist. (*C*) SRS image targeting the central 2,133 cm^{-1} vibrational peak of C–D shows no signal from live HeLa cells growing in regular medium. (*D*) SRS image targeting the 2,133 cm^{-1} vibrational peak of C–D exhibits weak but detectable contrast for live HeLa cells growing in a medium containing leucine-d_{10} (0.8 mM) for 20 h. (*E*) SRS image of the same cells as in *D* is background free when taken at an off-resonance frequency of 2,000 cm^{-1}. (*F*) SRS image of the same cells as in *D* at frequency of 2,940 cm^{-1} (CH_3 stretching attributed mainly to proteins) shows a much stronger signal from the total protein pool than the 2,133 cm^{-1} signal in *D*, but with similar protein distribution pattern.

leucine-d_{10} (Fig. 2*D*) shows a weak but clearly identifiable contrast outlining the cell shape. As a control, the off-resonant SRS image at 2,000 cm^{-1} of the same cells is background free (Fig. 2*E*). Such clean chemical contrast among Fig. 2 *C*–*E* would be difficult for CARS microscopy due to the presence of its nonresonant background. As a protein reference, an image taken at 2,940 cm^{-1} [CH_3 stretching mainly from proteins with minor cross talk from lipids (33)] shows both existing and newly synthesized proteins (Fig. 2*F*), the signal of which comes from the same regions but is much stronger than that in Fig. 2*D*. Thus, we have demonstrated the feasibility of using SRS imaging to detect newly synthesized proteins by specifically targeting the C–D vibrational signal of metabolically incorporated leucine-d_{10} in live HeLa cells. This opens up an imaging opportunity to capture nascent proteome dynamics in live cells under a myriad of cues.

Imaging Optimization by Metabolic Incorporation of a Deuterium-Labeled Set of All Amino Acids in Live HeLa Cells with Multicolor SRS Imaging. Although leucine is the most abundant essential amino acid, it only accounts for a small fraction of amino acids in proteins. Hence, we reasoned that deuterium labeling of all of the amino acids would lead to a substantial signal enhancement. Indeed, the spontaneous Raman spectrum (Fig. 3*A*) of HeLa cells incubated with a deuterium-labeled set of all 20 amino acids (prepared by supplying a uniformly deuterium-labeled whole set of amino acids to leucine-, lysine-, and arginine-deficient DMEM; for more details, refer to *Materials and Methods*) exhibits C–D vibrational peaks about five times higher than the blue spectrum in Fig. 2*B* under the same condition. The corresponding SRS image at 2,133 cm^{-1} (Fig. 3*B*) shows a significantly more pronounced signal than that in Fig. 2*D* under the same intensity scale. In particular, nucleoli (indicated by arrows in Fig. 3*B* and verified by differential interference contrast visualization) exhibit the highest signal, which is in accordance with previous reports using BONCAT and our own fluorescence staining results (Fig. S2). Nucleoli, the active sites for ribosomal biogenesis, have been reported to involve rapid nucleolar assembly and proteomic exchange (44–46). Such fast protein turnover is indeed reflected by the spatial enrichment of newly synthesized protein signals in those subcellular areas (Fig. 3*B*). Note that SRS imaging here is directly performed on live cells and hence free from potential complications due to fixation and dye conjugation. Again, the off-resonant image at 2,000 cm^{-1} is clean and dark (Fig. 3*C*), proving the specificity of SRS imaging of C–D at 2,133 cm^{-1}. In addition to imaging newly synthesized proteins, SRS can readily image intrinsic biomolecules in a label-free manner. By simply adjusting the energy difference between the Pump and the Stokes beams to match the vibrational frequency of amide I, lipids, and total proteins, respectively, Fig. 3 *D*–*F* shows the SRS images of amide I band at 1,655 cm^{-1} primarily attributed to proteins; CH_2 stretching at 2,845 cm^{-1} predominantly for lipids; and CH_3 stretching at 2,940 cm^{-1} mainly from proteins with minor contribution from lipids.

Time-Dependent de Novo Protein Synthesis and Protein Synthesis Inhibition. Being linearly dependent on analyte concentration, SRS contrast is well suited for quantification of de novo protein synthesis in live cells. Here, we show time-dependent protein synthesis images under the same intensity scale (Fig. 4 *A*–*C*). As expected, the new protein signal (2,133 cm^{-1}) from 5-, 12-, and 20-h incubation increases substantially over time (Fig. 4 *A*–*C*), whereas the amide I (1,655 cm^{-1}) signal remains at a steady state (Fig. 4 *D*–*F*). Because protein distribution is often heterogeneous in biological systems, we presented a more quantitative representation by acquiring ratio images between the newly synthesized proteins and the total proteome (from either amide I or CH_3). Fig. 4 *G*–*I* depicts the fraction of newly synthesized proteins (2,133 cm^{-1}) among the total proteome (1,655 cm^{-1}) and its spatial distribution. The fraction of newly synthesized proteins is growing with time from 5 to 20 h, gradually highlighting nucleoli as the subcellular compartments with fast protein turnover (44–46). Such quantitative ratio imaging of new versus old proteomes would be very difficult to obtain using BONCAT or mass spectroscopy without the destruction of cells. More time-dependent cell images are shown in Fig. S3. Moreover, Fig. 4*J* shows time-lapse SRS images of a live dividing HeLa cell after

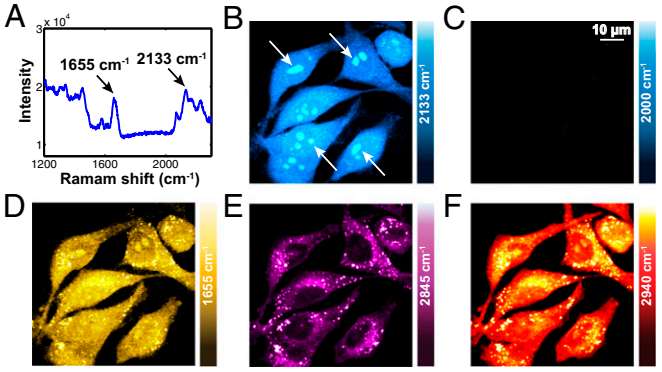

Fig. 3. SRS imaging of newly synthesized proteins by metabolic incorporation of a deuterium-labeled set of all amino acids in live HeLa cells. (*A*) Spontaneous Raman spectrum of HeLa cells incubated with a medium containing a deuterium-labeled set of all amino acids for 20 h, showing an approximately five times stronger peak at 2,133 cm^{-1} than the blue spectrum in Fig. 2*B*. (*B*) SRS image targeting the central 2,133 cm^{-1} vibrational peak of C–D shows a high-contrast image representing newly synthesized proteins. The same intensity scale bar is used here as in Fig. 2*D*. Consistent with previous reports, nascent proteins are distributed with a higher percentage in nucleoli (indicated by arrows), which are the active sites for ribosome biogenesis involving rapid import and degradation of proteins. (*C*) SRS image of the same cells as in *B* at off-resonance frequency 2,000 cm^{-1} is background free. (*D*–*F*) SRS images of same cells as in *B* at frequency of 1,655 cm^{-1} (amide I stretching attributed primarily to proteins), 2,845 cm^{-1} (CH_2 stretching attributed mainly to lipids), and 2,940 cm^{-1} (CH_3 stretching attributed mainly to proteins) show the intrinsic distributions of total cellular lipids and proteins.

20-h incubation in deuterium-labeled, all-amino acids medium, clearly proving the viability of cells under the imaging condition.

The effect of protein synthesis inhibition by chemical drugs is further tested to validate that the detected C–D signal indeed derives from nascent proteins. HeLa cells incubated with a deuterium-labeled set of all amino acids together with 5 μM anisomycin, which works as a protein synthesis inhibitor by inhibiting peptidyl transferase or the 80S ribosome system, for 12 h show the absence of the C–D signal in the spontaneous Raman spectrum (Fig. 4*K*). Furthermore, SRS imaging of the same samples (Fig. 4*L*) exhibits drastically weaker signal [Fig. S4 provides a more thorough analysis of the residual signal, which is possibly attributed to the intracellular free amino acid pool (47)] compared with Fig. 4*B* without the protein synthesis inhibitor. As a control, the corresponding 2,940 cm^{-1} image (Fig. 4*M*) of total proteome remains at a similar level as the non–drug-treated counterpart in Fig. 3*F*. Thus, the detected C–D SRS signal (Fig. 4 *A*–*C*) originates from deuterium-labeled nascent proteins, which vanishes upon adding the protein synthesis inhibitor.

Demonstration on HEK293T Cells and Neuron-Like Differentiable Neuroblastoma N2A Cells. To show the general applicability and potential of our method, we choose two additional mammalian cell lines for further demonstration: human embryonic kidney HEK293T cells, and neuron-like neuroblastoma mouse N2A cells, which can be induced to differentiate with the growth of neurites (i.e., axons and dendrites). The spontaneous Raman spectrum (Fig. 5*A*) of HEK293T cells incubated with a deuterium-labeled set of all amino acids for 12 h exhibits a 2,133 cm^{-1} C–D channel signal nearly as high as the 1,655 cm^{-1} amide channel signal. The resulting SRS image shows a bright signal for new proteins with an intense pattern residing in nucleoli (Fig. 5*B*). As before, the off-resonant image (2,000 cm^{-1}) displays vanishing background (Fig. 5*C*); the amide I channel (1,655 cm^{-1}) image (Fig. 5*D*) exhibits consistent overall proteome distributions similar to that in HeLa cells; CH_2 channel (2,845 cm^{-1}) image (Fig. 5*E*) depicts a more diffusive lipid distribution in cytoplasm compared with that in HeLa cells. Consistent with the results obtained in HeLa cells above, the ratio image (Fig. 5*F*) between the newly synthesized proteins (Fig. 5*B*) and the total proteins (Fig. 5*D*) highlights nucleoli for active protein turnover in HEK293T cells as well (44–46).

In addition to showing the ability to image newly synthesized proteins inside cell body, our technique can also be applied to tackle more complex problems, such as de novo protein synthesis in neuronal systems (2–4). As an initial demonstration, we imaged the newly synthesized proteins in neuron-like N2A cells, which have been extensively used as a model system to study neuronal differentiation, axonal growth, and signaling pathways. Under differentiation condition, N2A cells massively grow new neurites from cell bodies and form connections with other cells. Fig. 6*A* shows the image of newly synthesized proteins after induction for differentiation, by simultaneously differentiating the N2A cells and supplying with the deuterium-labeled set of all amino acids for 24 h. Similar to HeLa and HEK293T cells, N2A cell bodies are observed to display high-level protein synthesis. More interestingly, newly synthesized proteins are also observed in a subset of, but not all neurites (Fig. 6 *A* and *B*), which implies that the observed neurites in Fig. 6*A* are newly grown under the differentiation condition. For a detailed visualization, Fig. 6 *C* and *D* shows the zoomed-in regions in the dashed squares in Fig. 6 *A* and *B*, respectively. A more comprehensive examination is illustrated by both the ratio image (Fig. 6*E*) between Fig. 6 *C* and *D* and the merged image (Fig. 6*F*) with the red channel designating new protein signal from Fig. 6*C* and the green channel designating total protein signal from Fig. 6*D*. On one hand, both the ratio image and the merged image highlight the neurites with higher percentage of new proteins (indicated by stars), implying these neurites are newly grown. On the other hand, from the merged image, there are some neurites (indicated by arrows) showing obvious signals in the green channel (total proteins) only

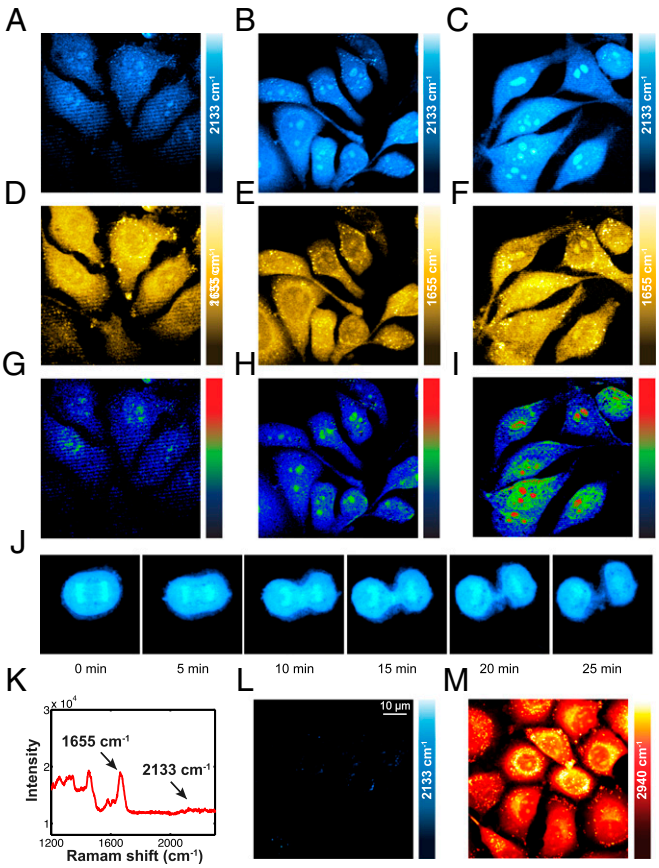

Fig. 4. SRS imaging of time-dependent de novo protein synthesis and drug-induced protein synthesis inhibition effect in live HeLa cells incubated in a deuterium-labeled all-amino acid medium. (*A*–*F*) SRS image targeting the central 2,133 cm^{-1} vibrational peak of C–D displays a time-dependent signal increase [5 h (*A*), 12 h (*B*), 20 h (*C*)] of the newly synthesized proteins, with nucleoli being gradually highlighted. As a control, the amide I (1,655 cm^{-1}) signal remains at a steady state over time [5 h (*D*), 12 h (*E*), 20 h (*F*)]. (*G*–*I*) Ratio images between the SRS image at 2,133 cm^{-1} (newly synthesized proteins) and the SRS image at 1,655 cm^{-1} (the amide I band from total proteins), representing the relative new protein fraction with subcellular resolution at each time point [5 h (*G*), 12 h (*H*), 20 h (*I*)]. The color bar ranging from black to red represents the ratio ranging from low to high. (*J*) Time-lapse SRS images of a live dividing HeLa cell during a 25-min time course after 20-h incubation with deuterated all-amino acids medium. (*K*) Spontaneous Raman spectrum of HeLa cells incubated with both deuterium-labeled all-amino acids and a protein synthesis inhibitor anisomycin (5 μM) for 12 h shows the drastic attenuation of the C–D Raman peak at 2,133 cm^{-1}. (*L*) SRS image of the same sample displays near vanishing signal throughout the whole field of view. (*M*) As a control, the image of the same cells at 2,940 cm^{-1} confirms that anisomycin does not influence the total protein level.

but with no detectable signal in the red channel (new proteins). Hence, the arrow indicated neurites are most likely older than their starred counterparts. In addition, the transition from green to red in the merged image (Fig. 6*F*) implies the growth direction by which new neurites form and grow. A second set of N2A images showing similar patterns as in Fig. 6 is also examined in Fig. S5. A more relevant system to study de novo protein synthesis and neuronal activities would be hippocampal neurons, which are known to be involved in long-term memory formation (2–4). SRS image (2,133 cm^{-1}) of hippocampal neuron cells incubated with a deuterium-labeled set of all amino acids shows a newly synthesized protein pattern in the neurites (Fig. S6). The intricate relationship between protein synthesis and neuronal activities is currently under investigation.

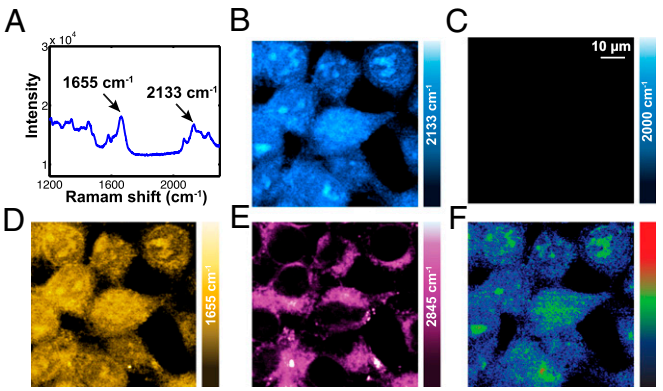

Fig. 5. SRS imaging of newly synthesized proteins by metabolic incorporation of a deuterium-labeled set of all amino acids in live human embryonic kidney (HEK293T) cells. (*A*) The spontaneous Raman spectrum of HEK293T cells incubated with a deuterium-labeled set of all amino acids for 12 h shows a 2,133 cm^{-1} C–D peak nearly as high as the amide I (1,655 cm^{-1}) peak. (*B*) SRS image targeting the central 2,133 cm^{-1} vibrational peak of C–D shows newly synthesized proteins in live HEK293T cells displaying a similar signal level as HeLa cells at 12 h (Fig. 4*B*). (*C*) As a comparison, the off-resonant image is still background free. (*D* and *E*) Multicolor SRS images of intrinsic cell molecules: total proteins [1,655 cm^{-1} (*D*)] and lipids [2,845 cm^{-1} (*E*)]. (*F*) The ratio image between new proteins (2,133 cm^{-1}) and total proteins (1,655 cm^{-1}) illustrates a spatial map for nascent protein distribution.

Conclusion

The ability to visualize newly synthesized proteomes in biological systems will greatly advance our understanding of complex cellular functions occurring in space and time (1–4). Currently, this endeavor is mainly pursued by several distinct contrast mechanisms including fluorescence staining, autoradiography, and mass spectroscopy. Here, we report a new technique of SRS microscopy coupled with stable isotope labeling (deuterium labeling in this study) to address this challenge. The major advantages of our technique lie in the following aspects. First, our approach is essentially noninvasive and completely compatible with the live-cell physiology. This is in contrast with earlier methods of autoradiography and BONCAT. In terms of sample preparations, the deuterium isotope has a high degree of similarity with the cells' endogenous counterpart (18–21). In terms of imaging conditions, SRS directly probes vibrational transitions in a stain-free manner using near-infrared lasers whose phototoxicity is low especially when using picosecond pulses. We note that a recent technique called multiisotope imaging mass spectrometry has also demonstrated a high-resolution isotope imaging ability (48, 49), but with a highly destructive nature due to the use of an ion microscope. Second, overcoming the major problems of CARS microscopy, SRS is an emerging nonlinear Raman microscopy with purely chemical contrast and high sensitivity, enabling fast imaging speed up to video rate in live animals and humans (41, 42). Our current electronics offers imaging speed of ~26 s per frame (512 × 512 pixels), which could be accelerated to video rate using a custom lock-in amplifier (33). As a comparison, spontaneous Raman microscopy relies on a feeble signal, which is easily overwhelmed by cell autofluorescence and needs long integration time (>hours) for imaging (23), and is thus undesirable for live-cell imaging. In fact, spontaneous Raman microscopy has been applied for detection of newly synthesized proteins, but was only possible with fixed cells (50). Third, SRS microscopy can readily offer the intrinsic total proteins distribution in a label-free manner. Such a valuable internal reference of total proteins is very hard to obtain for techniques such as BONCAT or mass spectroscopy without destruction of the cells.

Therefore, we have demonstrated SRS microscopy coupled with deuterium-labeled amino acids incorporation as an imaging technique for visualization of newly synthesized proteins in living mammalian cells under physiological conditions without any fixation or staining. From the perspective of biological applications, the biocompatiblility of both deuterium labeling and SRS imaging renders this technique the prospect of revealing spatial–temporal proteome dynamics in more complex systems such as live animals. From the perspective of imaging technology, nonlinear vibrational microscopy is well suited for visualizing the metabolic incorporation of isotope labeled precursors of macromolecules for its high sensitivity, specificity, and the non-invasive nature. We expect this strategy to be generalized and expanded to other stable isotopes such as ^{13}C and ^{15}N.

Materials and Methods

SRS Microscopy. The experimental setup is shown in Fig. 1*B*. Spatially and temporally overlapped pulsed Pump (tunable from 720 to 990 nm, 7 ps, 80-MHz repetition rate) and Stokes (1,064 nm, 5~6 ps, 80-MHz repetition rate, modulated at 10 MHz) beams, which are provided by picoEMERALD from Applied Physics & Electronics are coupled into an inverted laser-scanning microscope (FV1000 MPE; Olympus) optimized for near-IR throughput. A 60× water objective (UPlanAPO/IR; 1.2 N.A.; Olympus) is used for all cell imaging. After passing through the sample, the forward going Pump and Stokes beams are collected in transmission by a high N.A. condenser and imaged onto a large area Si photodiode. A high OD bandpass filter (890/220, Chroma) is used to block the Stokes beam completely and to transmit the Pump beam only for the detection of the stimulated Raman loss signal. The output current from the photodiode is terminated, filtered, and demodulated by a lock-in amplifier (SR844; Stanford Research Systems) at 10 MHz to ensure shot noise-limited detection sensitivity. For imaging, 512 × 512 pixels are acquired for one frame (26 s per frame) with a 100-μs pixel dwell time and 20-μs time constant from the lock-in amplifier. Powers after 60× IR objective used for imaging are as follows: 61 mW for modulated Stokes beam; 145 mW for the Pump beam of 2,133 cm^{-1}, 2,000 cm^{-1},

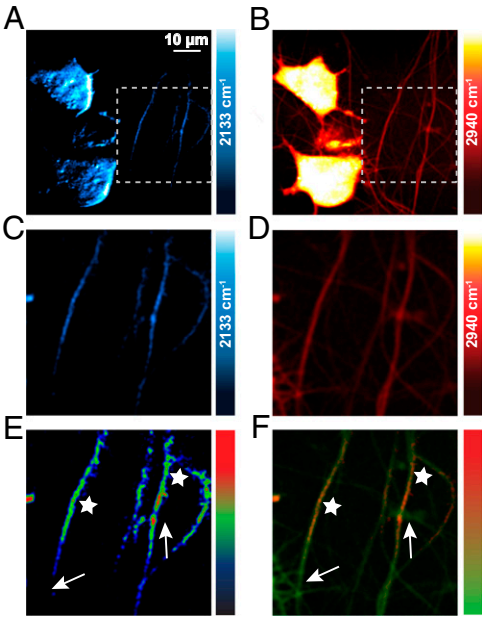

Fig. 6. SRS imaging of newly synthesized proteins in both cell bodies and newly grown neurites of neuron-like differentiable mouse neuroblastoma (N2A) cells. During the cell differentiation process by serum deprivation and 1 μM retinoic acid, deuterium-labeled all-amino acids medium is also supplied for 24 h. (*A*) SRS images targeting the 2,133 cm^{-1} peak of C–D show newly synthesized proteins. (*B*) SRS images targeting the 2,940 cm^{-1} CH_3 show total proteins. (*C* and *D*) Zoomed-in images as indicated in the white dashed squares in *A* and *B*. (*E*) Ratio image between new protein (*C*) and total proteins (*D*). Although the starred neurites show high percentage of new proteins, the arrows indicate neurites displaying very low new protein percentage. (*F*) Merged image between new protein (*C*) (red channel) and total proteins (*D*) (green channel). Similarly, the starred regions show obvious new proteins, whereas the arrows indicate regions that have undetectable new protein signal.

and 1,655 cm^{-1} channels; and 64 mW for Pump beam of 2,950 cm^{-1} and 2,845 cm^{-1} channels.

Metabolical Labeling of the Newly Synthesized Proteins by Deuterium-Labeled Amino Acids. Deuterium-labeled leucine-d_{10} medium is made by adding leucine-d_{10} (0.8 mM), lysine (0.8 mM), and arginine (0.4 mM) (Sigma) into leucine-, lysine-, and arginine-deficient DMEM (Sigma). Deuterium-labeled all-amino acids medium is made by adding uniformly deuterium-labeled amino acid mix (20 aa) (Cambridge Isotope) into leucine-, lysine-, and arginine-deficient DMEM (Sigma). The final concentration of leucine-d_{10} is adjusted to be 0.8 mM among the amino acid mix. (Because the starting medium is leucine, lysine, and arginine deficient, by adding the deuterium-labeled 20-aa mix, we essentially deuterate all of the leucine, lysine, and arginine as well as about one-half of the other amino acids.) Cells are seeded on a coverslip in a petri dish with 2 mL of regular DMEM with 10% (vol/vol) FBS and 1% penicillin/streptomycin (Invitrogen) for 20 h. The regular medium is then replaced with medium containing either leucine-d_{10} or a deuterium-labeled set of all amino acids. After incubation for a certain amount of time, the coverslip is taken out to make an imaging chamber filled with PBS for SRS imaging. For N2A cells, in the process of induced cell differentiation with serum deprivation and 1 μM retinoic acid, the deuterium-labeled set of all amino acids is supplemented.

Spontaneous Raman Spectroscopy. The spontaneous Raman spectra were acquired using a laser Raman spectrometer (inVia Raman microscope; Renishaw) at room temperature. A 27-mW (after objective), 532-nm diode laser was used to excite the sample through a 50×, N.A. 0.75 objective (NPLAN EPI; Leica). The total data acquisition was performed during 80 s using the WiRE software.

ACKNOWLEDGMENTS. We thank F. Hu, Z. Chen, V. W. Cornish, D. Peterka, and R. Yuste for helpful discussion. We are grateful to S. Buffington, M. Costa-Mattioli, and M. Sakamoto for providing hippocampal neurons, and Y. Li for his assistance on the spontaneous Raman microscope. We acknowledge support from Ellison Medical Foundation fellowships (to M.C.W.) and National Institutes of Health Director's New Innovator Award (to W.M.).

1. Hershey JWB, Sonenberg N, Mathews MB, eds (2012) *Protein Synthesis and Translational Control* (Cold Spring Harbor Lab Press, Cold Spring Harbor, NY).
2. Martin KC, Barad M, Kandel ER (2000) Local protein synthesis and its role in synapse-specific plasticity. *Curr Opin Neurobiol* 10(5):587–592.
3. Kandel ER (2001) The molecular biology of memory storage: A dialogue between genes and synapses. *Science* 294(5544):1030–1038.
4. Ho VM, Lee JA, Martin KC (2011) The cell biology of synaptic plasticity. *Science* 334(6056):623–628.
5. Chalfie M, Tu Y, Euskirchen G, Ward WW, Prasher DC (1994) Green fluorescent protein as a marker for gene expression. *Science* 263(5148):802–805.
6. Tsien RY (1998) The green fluorescent protein. *Annu Rev Biochem* 67:509–544.
7. Dieterich DC, Link AJ, Graumann J, Tirrell DA, Schuman EM (2006) Selective identification of newly synthesized proteins in mammalian cells using bioorthogonal noncanonical amino acid tagging (BONCAT). *Proc Natl Acad Sci USA* 103(25):9482–9487.
8. Beatty KE, et al. (2006) Fluorescence visualization of newly synthesized proteins in mammalian cells. *Angew Chem Int Ed Engl* 45(44):7364–7367.
9. Beatty KE, Tirrell DA (2008) Two-color labeling of temporally defined protein populations in mammalian cells. *Bioorg Med Chem Lett* 18(22):5995–5999.
10. Roche FK, Marsick BM, Letourneau PC (2009) Protein synthesis in distal axons is not required for growth cone responses to guidance cues. *J Neurosci* 29(3):638–652.
11. Dieterich DC, et al. (2010) In situ visualization and dynamics of newly synthesized proteins in rat hippocampal neurons. *Nat Neurosci* 13(7):897–905.
12. Tcherkezian J, Brittis PA, Thomas F, Roux PP, Flanagan JG (2010) Transmembrane receptor DCC associates with protein synthesis machinery and regulates translation. *Cell* 141(4):632–644.
13. Hinz FI, Dieterich DC, Tirrell DA, Schuman EM (2012) Non-canonical amino acid labeling in vivo to visualize and affinity purify newly synthesized proteins in larval zebrafish. *ACS Chem Neurosci* 3(1):40–49.
14. Liu J, Xu Y, Stoleru D, Salic A (2012) Imaging protein synthesis in cells and tissues with an alkyne analog of puromycin. *Proc Natl Acad Sci USA* 109(2):413–418.
15. Boyce M, Bertozzi CR (2011) Bringing chemistry to life. *Nat Methods* 8(8):638–642.
16. Schoenheimer R, Rittenberg D (1935) Deuterium as an indicator in the study of intermediary metabolism. *J Biol Chem* 111(1):163–168.
17. Schoenheimer R, Rittenberg D (1938) Application of isotopes to the study of intermediary metabolism. *Science* 87(2254):221–226.
18. Ong SE, et al. (2002) Stable isotope labeling by amino acids in cell culture, SILAC, as a simple and accurate approach to expression proteomics. *Mol Cell Proteomics* 1(5):376–386.
19. Mann M (2006) Functional and quantitative proteomics using SILAC. *Nat Rev Mol Cell Biol* 7(12):952–958.
20. Harsha HC, Molina H, Pandey A (2008) Quantitative proteomics using stable isotope labeling with amino acids in cell culture. *Nat Protoc* 3(3):505–516.
21. Geiger T, et al. (2011) Use of stable isotope labeling by amino acids in cell culture as a spike-in standard in quantitative proteomics. *Nat Protoc* 6(2):147–157.
22. Ingolia NT, Lareau LF, Weissman JS (2011) Ribosome profiling of mouse embryonic stem cells reveals the complexity and dynamics of mammalian proteomes. *Cell* 147(4):789–802.
23. Potma EO, Xie XS (2008) Theory of spontaneous and coherent Raman scattering. *Handbook of Biomedical Nonlinear Optical Microscopy*, eds Masters BR, So PTC (Oxford Univ Press, New York).
24. Zumbusch A, Holtom GR, Xie XS (1999) Three-dimensional vibrational imaging by coherent anti-Stokes Raman scattering. *Phys Rev Lett* 82(20):4142–4145.
25. Evans CL, Xie XS (2008) Coherent anti-stokes Raman scattering microscopy: Chemical imaging for biology and medicine. *Annu Rev Anal Chem (Palo Alto Calif)* 1:883–909.
26. Cheng JX, Xie XS (2004) Coherent anti-Stokes Raman scattering microscopy: Instrumentation, theory, and applications. *J Phys Chem B* 108(3):827–840.
27. Pezacki JP, et al. (2011) Chemical contrast for imaging living systems: Molecular vibrations drive CARS microscopy. *Nat Chem Biol* 7(3):137–145.
28. Suhalim JL, Boik JC, Tromberg BJ, Potma EO (2012) The need for speed. *J Biophotonics* 5(5–6):387–395.
29. Ploetz E, Laimgruber S, Berner S, Zinth W, Gilch P (2007) Femtosecond stimulated Raman microscopy. *Appl Phys B* 87(3):389–393.
30. Freudiger CW, et al. (2008) Label-free biomedical imaging with high sensitivity by stimulated Raman scattering microscopy. *Science* 322(5909):1857–1861.
31. Ozeki Y, Dake F, Kajiyama S, Fukui K, Itoh K (2009) Analysis and experimental assessment of the sensitivity of stimulated Raman scattering microscopy. *Opt Express* 17(5):3651–3658.
32. Nandakumar P, Kovalev A, Volkmer A (2009) Vibrational imaging based on stimulated Raman scattering microscopy. *New J Phys* 11:033026.
33. Saar BG, et al. (2010) Video-rate molecular imaging in vivo with stimulated Raman scattering. *Science* 330(6009):1368–1370.
34. Zhang D, Slipchenko MN, Cheng JX (2011) Highly sensitive vibrational imaging by femtosecond pulse stimulated Raman loss. *J Phys Chem Lett* 2(11):1248–1253.
35. Wang MC, Min W, Freudiger CW, Ruvkun G, Xie XS (2011) RNAi screening for fat regulatory genes with SRS microscopy. *Nat Methods* 8(2):135–138.
36. Zhang X, et al. (2012) Label-free live-cell imaging of nucleic acids using stimulated Raman scattering microscopy. *ChemPhysChem* 13(4):1054–1059.
37. Fu D, et al. (2012) Quantitative chemical imaging with multiplex stimulated Raman scattering microscopy. *J Am Chem Soc* 134(8):3623–3626.
38. Ozeki Y, et al. (2012) High-speed molecular spectral imaging of tissue with stimulated Raman scattering. *Nat Photonics* 6:845–851.
39. Einstein A (1917) On the quantum theory of radiation. *Phys Z* 18:121–128.
40. Bloembergen N (1967) The stimulated Raman effect. *Am J Phys* 35(11):989–1023.
41. Min W, Freudiger CW, Lu S, Xie XS (2011) Coherent nonlinear optical imaging: Beyond fluorescence microscopy. *Annu Rev Phys Chem* 62:507–530.
42. Min W (2011) Label-free optical imaging of nonfluorescent molecules by stimulated radiation. *Curr Opin Chem Biol* 15(6):831–837.
43. Okayasu T, Ikeda M, Akimoto K, Sorimachi K (1997) The amino acid composition of mammalian and bacterial cells. *Amino Acids* 13(3-4):379–391.
44. Phair RD, Misteli T (2000) High mobility of proteins in the mammalian cell nucleus. *Nature* 404(6778):604–609.
45. Andersen JS, et al. (2005) Nucleolar proteome dynamics. *Nature* 433(7021):77–83.
46. Boisvert FM, et al. (2012) A quantitative spatial proteomics analysis of proteome turnover in human cells. *Mol Cell Proteomics* 11(3):M111.011429.
47. Piez KA, Eagle H (1958) The free amino acid pool of cultured human cells. *J Biol Chem* 231(1):533–545.
48. Lechene CP, Luyten Y, McMahon G, Distel DL (2007) Quantitative imaging of nitrogen fixation by individual bacteria within animal cells. *Science* 317(5844):1563–1566.
49. Zhang DS, et al. (2012) Multi-isotope imaging mass spectrometry reveals slow protein turnover in hair-cell stereocilia. *Nature* 481(7382):520–524.
50. van Manen HJ, Lenferink A, Otto C (2008) Noninvasive imaging of protein metabolic labeling in single human cells using stable isotopes and Raman microscopy. *Anal Chem* 80(24):9576–9582.